Chronic Sleep Fragmentation Enhances Habenula Cholinergic Neural Activity

Feifei Ge[1,2], **Ping Mu**[1,3], **Rong Guo**[1], **Li Cai**[1], **Zheng Liu**[1], **Yan Dong**[1,4], **Yanhua H. Huang**[1]

[1]Department of Psychiatry, University of Pittsburgh, Pittsburgh, PA

[2]Present address: Department of Human Anatomy and Histoembryology, School of Medicine and Life Sciences, Nanjing University of Chinese Medicine, Nanjing, 210023, China

[3]Present address: College of Life Sciences, Ludong University, 186 Hongqi Middle Road, Yantai, Shandong, 264025, China

[4]Department of Neuroscience, University of Pittsburgh, Pittsburgh, PA

Abstract

Sleep is essential to emotional health. Sleep disturbance, particularly REM sleep disturbance, profoundly impacts emotion regulation, but the underlying neural mechanisms remain elusive. Here we show that chronic REM sleep disturbance, achieved in mice by chronic sleep fragmentation (SF), enhanced neural activity in the medial habenula (mHb), a brain region increasingly implicated in negative affect. Specifically, after a 5-day SF procedure that selectively fragmented REM sleep, cholinergic output neurons (ChNs) in the mHb exhibited increased spontaneous firing rate and enhanced firing regularity in brain slices. The SF-induced firing changes remained intact upon inhibition of glutamate, GABA, acetylcholine, and histamine receptors, suggesting cell-autonomous mechanisms independent of synaptic transmissions. Moreover, the SF-induced hyperactivity was not because of enhanced intrinsic membrane excitability, but was accompanied by depolarized resting membrane potential in mHb ChNs. Furthermore, inhibition of TASK-3 (KCNK9) channels, a subtype of two-pore domain K^+ channels, mimicked the SF effects by increasing the firing rate and regularity, as well as depolarizing the resting membrane potential in mHb ChNs in control-sleep mice. These effects of TASK-3 inhibition were absent in SF mice, suggesting reduced TASK-3 activity following SF. By contrast, inhibition of small-conductance Ca^{2+}-activated K^+ (SK) channels did not produce similar effects. Thus, SF compromised TASK-3 function in mHb ChNs, which likely led to depolarized resting membrane potential and increased spontaneous firing. These results not only demonstrate that selective REM sleep disturbance leads to hyperactivity of mHb ChNs, but also identify a key molecular substrate through which REM sleep disturbance may alter affect regulation.

Corresponding Address: Dr. Y.H. Huang, 450 Technology Dr., Pittsburgh, PA 15219, yhhuang@pitt.edu, Phone: 412-624-7581.

Keywords

sleep fragmentation; habenula; cholinergic; TASK-3; KCNK9; treadmill

---

Introduction

Sleep disturbance is a risk factor for a range of psychiatric conditions, including anxiety, depression, and drug addiction[1–6]. A key mechanistic argument is sleep-regulation of emotion[7–10]. Deficient sleep, especially REM sleep disturbance, impairs both positive and negative affect and distorts emotional brain reactivity[8, 9, 11]. Moreover, a number of brain regions that regulate emotion processing are affected by deficient sleep[8, 11–13]. However, the molecular, cellular, and circuit mechanisms by which sleep disturbance impacts affect regulation are not well understood.

The medial habenula complex (mHb) in the epithalamus is increasingly recognized for mood regulations[14]. It receives inputs from limbic forebrain, and feeds to midbrain monoaminergic centers via the interpeduncular nucleus (IPN)[14]. The mHb-to-IPN projections are predominantly cholinergic, whose activity regulates various affect-associated behaviors including stress, fear, anxiety, memory, and drug-relapse[15–21]. The mHb cholinergic neurons (ChNs) are tonically active, and respond to a wide range of neurotransmitters and neuromodulators[14]. However, it is not known whether and how mHb ChNs may be affected by sleep disturbance.

Here we show that following a 5-day chronic sleep fragmentation (SF) procedure that resulted in selective REM sleep disturbance, mHb ChNs exhibited an increase in the tonic firing rate, which was at least in part mediated by dampened activity of the two-pore domain K^+ channel (K_{2P}) TWIK-like acid-sensitive K^+ channel 3 (TASK-3, also named KCNK9). These results reveal a key molecular and cellular substrate through which sleep disturbance may impact affect regulation.

Materials and Methods

Animals

ChAT^{BAC}-EGFP mice (Jackson Laboratory, stock # 007902)[22] of both males and females, 6–16 weeks old, were used at the beginning of the experiments. Mice were maintained at room temperature ($22 \pm 1°C$), controlled humidity ($60 \pm 5\%$), under a 12:12-h light/dark cycle (lights on at 7:00 am, off at 7:00 pm), and individually housed with constant access to food and water. Mice usage was in accordance with protocols approved by the Institutional Animal Care and Use Committee at the University of Pittsburgh.

Sleep Fragmentation

Mice were singly housed in custom-made treadmill boxes measured 14 cm x 30 cm x 15 cm (ITCC Life Science)[23] with flexible stainless steel mesh floor covered with normal bedding. A cylinder-shaped object (~1.5 cm in height) was fixed to the treadmill belt underneath and quietly moved bidirectionally with the belt across the entire mesh floor (Fig. 1A). Movement

of the object underneath the mesh floor prevented the mice from having undisturbed sleep (Fig. 1D), without engaging consistent gross movement of the mice. The treadmills were programmed to move at the speed of ~2.3 cm/sec in alternating directions throughout the light and dark phases. For partial-SF group ($SF_{partial}$), mice were subjected to continuous treadmill belt movement for 1 hr followed by a 2-hr rest, repeated throughout the 24 hr. All treadmill procedures lasted for 5–7 days. "Control-sleep" mice were housed in similar boxes without movement of the treadmill belts. All mice housed in these boxes had access to food and water ad libitum.

EEG surgery, recordings and analysis

A group of 6 mice was used for EEG/EMG recordings. Surgery for installing EEG apparatus was similar as described previously[24, 25]. Briefly, two stainless-steel wire electromyogram (EMG) electrodes were inserted into the nuchal neck muscle and two gold-plated wire EEG electrodes (Plastics One, Roanoke, VA) were installed contralaterally through the skull over the parietal and frontal cortices. Electrode leads were gathered into a plastic socket (Plastics One) and fixed to the skull with dental cement. Mice were allowed to recover for ~10 days before experimentation. All mice were singly housed post-surgery and during subsequent experimentation.

EEG and EMG electrodes were connected to the amplifiers via lightweight cables and commutators (Plastics One). Mice were allowed to habituate for 3–6 days before data collection. EEG and EMG signals were amplified using Grass model 15LT bipolar amplifiers (Grass Technologies, West Warwick, RI) and an analog-digital converter (Kissei Comtec). The EEG was filtered below 0.1 Hz and above 100 Hz. The EMG was filtered below 30 Hz and above 3 kHz. All signals were digitized at 128 Hz and collected using Vital Recorder software (Kissei Comtec, Nagano, Japan). All signals were manually scored for sleep states in 10-sec epochs using Sleep Sign for Animal software (Kissei Comtec, Nagano, Japan). Wakefulness was identified by desynchronized EEG and high EMG activity; NREM sleep exhibited high amplitude slow waves and lower EMG; REM sleep exhibited regular EEG theta activity and extremely low EMG activity (Fig. 1C *top*). Consolidated sleep durations were determined by the same sleep states in a stretch of time of no less than 20 sec (2 epochs). For EEG power spectrum analysis, EEG signals underwent Fast Fourier Transformation using 0.5 Hz frequency bin, and were normalized to the average delta power (0–4 Hz, for NREM) or theta power (5–10 Hz, for REM) of the baseline condition (prior to SF). All mice were coded for sleep scoring, and then decoded for data compiling.

Plasma corticosterone assay

Four groups of mice (n = 7–9/group) singly housed in the same conditions were used for this assay. The control-sleep, $SF_{partial}$, and SF groups underwent procedures as described above. All three groups had 20-min wakeful time after 1:00 pm before blood sampling. A fourth group was subjected to acute physical restraint for 30 min in mouse restrainers before blood sampling, which served as positive stress controls. All blood samples were collected at the same time of the day around 1:30 – 2:00 pm. The mice were decapitated after isoflurane anesthesia, and trunk blood was collected in heparin-containing tubes. Samples were kept on ice for <30 min before centrifuged at 1500 x g at 4°C for 10 min. The supernatant was stored

at −80°C for later analysis. Plasma corticosterone concentrations were determined by Corticosterone ELISA Kit (Enzo Life Sciences).

Immunohistochemistry

The mouse was anesthetized with overdosed isoflurane, and then perfused transcardially with 0.1 M phosphate buffer (PB) followed by 4% paraformaldehyde in PB. Brains were removed carefully and given an additional overnight postfix in 4% paraformaldehyde at 4°C, and then transferred to 30% sucrose in PB for 48 hr before sectioning. Coronal sections (35 μm) were cut on a cryostat (Leica CM1950), rinsed in 0.1 M PB, incubated in PB containing 0.5% sodium borohydride (30 min), rinsed, incubated in PB containing 0.5% H_2O_2 (15 min), and rinsed again. Primary and secondary antisera were diluted in PB containing 1% normal donkey serum (Jackson ImmunoResearch, West Grove, PA) and 0.3% Triton X-100 (Sigma). Sections were incubated with the primary antibody (polyclonal goat anti-choline acetyltransferase, AB144P, 1:200; Millipore Sigma) in the blocking solution overnight at room temperature. After rinsing, the sections were incubated with the secondary antibody (Alexa Fluor 594-conjugated donkey anti-goat IgG, 1:500; Abcam) for 90 min at room temperature, and mounted using Fluoromount-G mounting medium (SouthernBiotech). Fluorescence images were taken under an Olympus IX71 fluorescence microscope at 4x or 10x original magnification, using QImaging camera and MetaMorph Advanced software.

RNAscope in situ hybridization

Single-molecule RNA fluorescent in situ hybridization was performed using RNAscope probes (ACDBio) according to the manufacturer's protocol. Fresh frozen mouse brain was sectioned at 10-μm thickness on a cryostat (Leica CM1950). Mouse Kcnk9 (TASK-3) probe (#475681) was used for detecting TASK-3, and DapB probe (#310043) was used as a negative control. Images were obtained from two consecutive sections probed with TASK-3 and DapB respectively, using the same exact camera settings under an Olympus IX71 fluorescence microscope at 10x or 40x original magnification.

mHb Slice Preparation

Acute mHb slices were prepared around 9:00–10:00 am. The mouse was deeply anesthetized with isoflurane and subsequently decapitated. The brain was removed and sliced using modified solutions to better preserve slice quality[26]. Briefly, coronal slices containing the mHb were cut at 200 μm thickness using a Leica VT1200s vibratome in 4°C cutting solution (in mM: 92 N-methyl-D-glucamine, 2.5 KCl, 1.2 NaH_2PO_4, 30 $NaHCO_3$, 20 HEPES, 0.5 $CaCl_2$, 10 $MgSO_4$, 25 glucose, 5 sodium ascorbate, 2 thiourea, and 3 sodium pyruvate, pH adjusted to 7.3 with HCl, osmolarity 305, and saturated with 95% O_2 /5% CO_2). Slices were transferred to 37°C cutting solution and kept for ~9 min, then transferred to oxygenated holding solution (in mM: 86 NaCl, 2.5 KCl, 1.2 NaH_2PO_4, 35 $NaHCO_3$, 20 HEPES, 2 $CaCl_2$, 1 $MgSO_4$, 25 glucose, 5 sodium ascorbate, 2 thiourea, and 3 sodium pyruvate, pH adjusted to 7.3, osmolarity 305, and saturated with 95% O_2 /5% CO_2) to allow for recovery at room temperature for ~1 hr before electrophysiological recordings.

For electrophysiological recordings, one slice was transferred each time from the holding chamber to a submerged recording chamber, where it was continuously superfused with

oxygenated artificial CSF (aCSF, in mM: 119 NaCl, 2.5 KCl, 1 NaH_2PO_4, 1.3 $MgCl_2$, 2.5 $CaCl_2$, 26.2 $NaHCO_3$, and 11 glucose, 290 mOsm, saturated with 95% O_2/5% CO_2) maintained at $31 \pm 1°C$. For pH experiments (**Fig. 5A**), HEPES-buffered aCSF (in mM: 130 NaCl, 3 KCl, 10 HEPES, 2.5 $MgCl_2$, 2.5 $CaCl_2$, 26.2 $NaHCO_3$, and 10 glucose, pH adjusted to 7.3, 7.0 and 6.5 with NaOH, 290 mOsm, saturated with 100% O_2) was used for recordings and maintained at $31 \pm 1°C$.

Electrophysiology

Slice recordings were performed between 11:00 am - 3:00 pm. Loose-patch or whole-cell recordings were made under visual guidance (40x, infrared Dodt contrast imaging) from EGFP^{+} neurons located in the ventral 2/3 of mHb (Fig. 2A). Loose-patch electrodes were filled with bathing aCSF, and access resistance was maintained at ~ 20–50 MΩ throughout the experiment. Whole-cell current-clamp electrodes were filled with a K^{+}-based internal solution (in mM: 108 K-methanesulfonate, 20 KCl, 10 HEPES, 0.4 EGTA, 2.0 $MgCl_2$, 2.5 MgATP, 0.25 Na_3GTP, 7.5 Na_2-phosphocreatine, 1 L-glutathione, pH 7.25–7.30; 290 mOsm). All signals were filtered at 2.6–3 KHz, amplified at 5x using a MultiClamp 700B amplifier (Molecular Device), and digitized at 20 KHz with a Digidata 1440A analog-to-digital converter (Molecular Devices). Histamine hydrochloride, TMPH hydrochloride, CGP 55845 hydrochloride, NBQX, D-AP5, SR 95531, dihydro-β-erythroidine hydrobromide, scopolamine, NS 309, UCL 1684, TRAM 39, and PK-THPP were purchased from *R&D Systems*, and all other reagents were obtained from *Sigma-Aldrich*.

Data Acquisition and Analysis

All data were analyzed without prior awareness of the treatment (control-sleep, SF_partial, SF, and SF recovery). A ~5 min baseline was recorded for each loose patch recordings, and ~1 min of continuous spontaneous action potential firing ~10–15 min following drug application was averaged for frequency analysis. For loose-patch recordings, changes in the access resistance may lead to changes in field potential amplitudes. This, however, did not affect the quantification of firing frequency, and therefore such results were included for frequency analyses. Loose-patch recordings were performed under either current-clamp mode with 0 holding current (Figs. 2 and 4) or voltage-clamp mode with 0 holding voltage (Figs. 3 and 5). Neither recording configuration perturbs spontaneous action potential firing. To obtain the resting membrane potential (RMP), at least 30 sec after forming a GΩ seal onto the cell membrane and immediately (< 5 sec) upon break-in, the membrane voltage was measured under whole-cell current-clamp mode with 0 holding current as a close approximate of RMP. All subsequent electrophysiological measurements were performed after stabilization (> 5 min) under whole-cell configuration. The input resistance (R_{in}) was measured by injecting a hyperpolarizing current of 10 pA at ~ −70 mV under whole-cell current-clamp mode. To assess membrane excitability, at least 5 min after achieving whole-cell configuration, a current-step protocol (from 10 to 130 pA with 300-ms step duration and 20-pA increment) was run and repeated. Action potential amplitude was defined as voltage change from the action potential threshold to peak, and the rise time was defined as the time elapsed for the action potential to rise from 10% to 90% of the full spike amplitude. Rheobase current was defined as the minimal current necessary to elicit action potential firing. The afterhyperpolarization potential (AHP) was measured upon rheobase current

injection following the first action potential spike, and defined as the maximal hyperpolarization relative to threshold at 2–5 ms following spike initiation (fast AHP; fAHP) or at 15–50 ms (medium AHP; mAHP; Table 1).

Statistics

Sample sizes for each of the experiments were based on previous studies or power analysis from pilot experiments. Animals were assigned randomly to treatment groups to balance age and sex where applicable. Each experiment was replicated in at least 5 mice unless otherwise specified. Numbers of cells (n) and animals (m) are presented as "n/m". Unless specified, "n" as the default sample size was used in all statistics. All results are shown using box-and-whiskers plots (in the style of Tukey) except in Fig. 2D and5E, where mean ± SEM data are shown as appropriate. All results (including outliers as shown in box-and-whiskers plots) were included for analyses, except in Fig. 4A, where 2 cells were excluded for firing interval analysis due to a complete suppression of firing in NS 309. Statistical analysis was performed using Prism GraphPad (version 7). Data were assumed normal distribution. Statistical significance was assessed using two-tailed t tests for two-group comparisons, one-way or one-way repeated measure (RM) ANOVAs, two-way or two-way RM ANOVAs, followed by Tukey, Dunnett, or Sidak post-hoc tests based on experimental designs and recommendations by Prism 7. $p < 0.05$ was considered statistically significant.

Results

Chronic SF in mice

To achieve chronic sleep disturbance in mice, we used a custom-made programmable treadmill system[23] to produce chronic SF (Fig. 1A; details see Methods). A legitimate concern is that our SF procedure may not only disturb sleep, but also cause stress and induce stress hormone-mediated consequences. To address this, we first determined the stress levels following our SF procedure by measuring the plasma corticosterone levels, a method commonly used to assess stress induced by various sleep manipulations[24, 27]. As shown in Fig. 1B, mice following 5 days of SF exhibited similar corticosterone levels as in control-sleep or SF$_{partial}$ groups, whereas mice receiving acute physical restraint stress (positive control) exhibited significantly higher corticosterone levels ($F_{(3, 28)} = 165.3$, $p < 0.0001$; SF, $p = 0.265$, 0.936 compared to control-sleep and SF$_{partial}$ respectively, stress group, $p < 0.001$ compared to all others; n = 7–9 each, one-way ANOVA with Tukey posttest). Furthermore, the corticosterone levels in sleep, SF$_{partial}$, and SF groups were all within the normal range typically observed in male mice around the same time of day[28]. These results suggest that our SF procedure induces minimal levels of stress.

To examine the efficacy of our SF procedure, we recorded EEG and EMG signals from mice under four experimental conditions (n = 6 each group; 5 days each condition): control-sleep, SF$_{partial}$, SF, and SF-recovery (see **Methods**). The SF procedure appears to be modest as it did not change the 24-hr total wakefulness, NREM, or REM sleep times (wakefulness, $F_{(3, 15)} = 0.548$, $p = 0.657$; NREM, $F_{(3, 15)} = 1.197$, $p = 0.335$; REM, $F_{(3, 15)} = 3.337$, $p = 0.048$, SF was not significantly different compared to other groups; one-way RM ANOVA with Tukey posttest; Fig. 1C). Furthermore, SF effectively reduced the average duration of

REM sleep episodes ($F_{(3, 15)}$ = 6.975, p = 0.004; SF, p = 0.016, 0.003 compared to control-sleep and SF-recovery, $SF_{partial}$ was not significantly different from any other groups; one-way RM ANOVA with Tukey posttest; Fig. 1D), and led to a trend increase in the number of transitions into REM sleep ($F_{(3, 15)}$ = 4.108, p = 0.026; SF, p = 0.056, 0.042 compared to control-sleep and SF-recovery, $SF_{partial}$ was not significantly different from any other groups; one-way RM ANOVA with Tukey posttest; Fig. 1E). These results demonstrate that our SF procedure effectively induced REM sleep fragmentation. On the other hand, SF slightly increased the average duration of wakefulness bouts but did not alter NREM sleep episode durations (wakefulness, $F_{(3, 15)}$ = 3.577, p = 0.039; SF, p = 0.006, 0.088 compared to control-sleep and SF-recovery; NREM, $F_{(3, 15)}$ = 2.577, p = 0.093; one-way RM ANOVA). SF also did not alter the number of transitions into wakefulness or NREM (wakefulness, $F_{(3, 15)}$ = 8.024, p = 0.002; SF, p = 0.193, 0.814 compared to control-sleep and SF-recovery; NREM, $F_{(3, 15)}$ = 6.885, p = 0.004; SF, p = 0.996, 0.080 compared to control-sleep and SF-recovery; one-way RM ANOVA with Tukey posttest; Fig. 1D,E). Finally, SF did not alter the power spectra of NREM or REM under the four sleep conditions (main effect of sleep: NREM, $F_{(3, 15)}$ = 0.537, p = 0.664; REM, $F_{(3, 15)}$ = 0.562, p = 0.587, one-way RM ANOVA; Fig. 1F). Thus, our SF procedure selectively impairs REM sleep in mice by inducing chronic REM sleep fragmentation.

SF enhances spontaneous firing of ChNs in mHb

The mHb is densely populated with ChNs[29, 30], which regulate negative affect mainly via the mHb-IPN projection (reviewed by[14]). We used a transgenic mouse line that expresses EGFP driven by choline acetyltransferase (ChAT) promoter (ChAT[BAC]-EGFP[22]), thus allowing fluorescence visualization of mHb ChNs in brain slices. Using ChAT immunoreactivity, we confirmed that EGFP[+] and ChAT^{+} neurons highly overlapped (100% of EGFP^{+} neurons were ChAT[+]; Fig. 2A). The dense expression of ChAT/EGFP in the ventral two-thirds of the mHb was also consistent with previous observations[15, 22, 29].

We therefore made loose-patch recordings from mHb EGFP^{+} neurons as ChNs in acute brain slices. ChNs in mHb slices exhibited tonic firing (Fig. 2B), consistent with previous reports[31, 32]. SF increased the frequency of spontaneous firing in mHb ChNs ($F_{(3, 99)}$ = 4.798, p = 0.004; SF compared to control-sleep, p = 0.002; one-way ANOVA with Tukey posttest), which was accompanied by a decrease in the coefficient of variation (CV) of firing intervals ($CV_{interval}$: $F_{(3, 99)}$ = 3.271, p = 0.024; SF compared to control-sleep, p = 0.016; one-way ANOVA with Tukey posttest; Fig. 2B), suggesting enhanced firing regularity. Importantly, this increase in spontaneous firing was only observed under loose-patch recordings, and was absent soon after achieving whole-cell configuration (control-sleep/$SF_{partial}$/SF, $F_{(2, 63)}$ = 0.238, p = 0.789, one-way ANOVA), suggesting the essential roles of cytosolic diffusible factors (e.g. intracellular K^+, pH, and G-protein signaling etc.) in the regulation. Furthermore, the increase in tonic firing was likely attributable to the more depolarized resting membrane potential following SF ($F_{(3, 91)}$ = 3.261, p = 0.025; SF compared to control-sleep, p = 0.027; one-way ANOVA with Tukey posttest; Fig. 2C), which was measured immediately (< 5 sec) after achieving whole-cell configuration, presumably before the wash-in saline-induced normalization of the membrane potential.

After stabilization under whole-cell current-clamp configuration (> 5 min), we normalized the resting membrane potential across groups and measured the intrinsic membrane excitability of mHb ChNs by injecting a series of current steps to evoke action potential firing. The action potential firing exhibited substantial frequency accommodation, which is typical for mHb neurons[33]. At low injecting currents (0–90 pA), the evoked firing rates were not different between any groups, and the frequency range (0–19 Hz) well covered the entire span of the basal firing frequency range (~0.5–10 Hz). At the highest injecting currents (110–130 pA), the evoked firing rates were lower in the SF group, suggesting reduced excitability (sleep x current interaction: $F_{(18, 462)} = 1.971$, $p = 0.010$; SF compared to control-sleep and SF-recovery, $p < 0.05$ and $p < 0.01$ at 110 and 130 pA current injections, two-way ANOVA with Tukey posttest; Fig. 2D). However, the evoked firing frequencies (~20–30 Hz) under high injecting currents were well above the basal firing range (~0.5–10 Hz), thus it is not likely that the SF-induced increase in basal firing rate is explained by changes in the intrinsic membrane excitability. Consistently, no changes were detected in any other parameters related to the membrane properties, including input resistance, action potential threshold/amplitude/kinetics, fast/medium after-hyperpolarizations, and rheobase current (Table 1). Thus, compared to the mainstream ion channels mediating the active membrane properties, cytosolic membrane modulators and resting conductances are more likely the substrates that mediate SF-induced membrane depolarization and elevated tonic firing in mHb ChNs.

Neurotransmitter receptors in SF-induced increase of tonic firing in mHb ChNs

The mHb receives a variety of neurotransmitter and neuromodulator inputs, including glutamatergic, GABAergic, histaminergic, cholinergic, dopaminergic, norepinephrine, purinergic, and possibly also serotonergic inputs[14]. All of these inputs are dynamically regulated by sleep-wakefulness cycles to modulate neural activity and orchestrate intracellular signaling. To probe along this line, we started by testing the wakefulness-promoting histamine signaling. ChNs in the basal forebrain and striatum express high levels of histamine receptors, which potently regulate membrane depolarization and action potential firing[34, 35]. In the rodent Hb, relatively low levels of histamine H2 and H3 receptors are expressed[36–38]. Application of histamine (10 μM) did not affect the spontaneous action potential firing frequency in mHb ChNs in control-sleep group or in SF group (SF x histamine interaction, $F_{(1, 11)} = 0.455$, $p = 0.514$; main effect of histamine: $F_{(1, 11)} = 1.431$, $p = 0.257$; Fig. 3A), nor did it change the firing regularity ($CV_{interval}$: SF x histamine interaction, $F_{(1, 11)} = 1.197$, $p = 0.297$; main effect of histamine: $F_{(1, 11)} = 0.999$, $p = 0.339$; two-way RM ANOVA with Sidak posttest). Thus, these results do not support a role of histamine signaling in regulating the tonic firing of mHb ChNs.

Next, we tested cholinergic signaling by focusing on nicotinic acetylcholine receptors (nAChRs). The vast majority of mHb neurons express high levels of nAChRs containing α3, α4, α5, β2, and/or β4[39], activation of which elicits a depolarizing current, enhances the membrane excitability, and increases the firing rate of these neurons[32, 33, 39]. We therefore tested whether nAChRs may mediate SF-induced increase in mHb ChNs firing. However, application of a non-competitive, pan-selective (i.e. α3, α4 and β2, β4) nAChR antagonist TMPH hydrochloride (1 μM) did not affect the tonic action potential firing rate in mHb

ChNs following SF ($p = 0.984$, n = 6/2, two-tailed paired t test; Fig.3B), a result unsupportive of the involvement of nAChR signaling.

Next, we tested $GABA_B$ receptors, which are highly enriched within rodent mHb[15, 40]. Activation of $GABA_B$ receptors at the soma-dendritic region hyperpolarizes mHb neurons and inhibits firing, although inhibition of $GABA_B$ receptors does not increase the basal firing, suggesting that mHb soma-dendritic $GABA_B$ receptors are not constitutively active under basal slice conditions[31]. On the other hand, activation of $GABA_B$ receptors located at the axon terminals of mHb ChNs elicits an unconventional, excitatory responses to facilitate neurotransmitter release[15]. To test whether a similar excitatory effect of $GABA_B$ receptor activation at the soma-dendritic region of mHb ChNs plays a role in SF-induced effects, we applied the $GABA_B$ receptor-selective antagonist CGP 55845 (1 μM), which, however, did not affect the tonic firing in mHb ChNs following SF ($p = 0.864$, n = 4/2, two-tailed paired t test; Fig. 3C). This result is thus unsupportive of the involvement of $GABA_B$ signaling.

Finally, we tested a cocktail of neurotransmitter receptor antagonists, including NBQX (5 μM) and D-AP5 (50 μM) to block glutamate AMPA and NMDA receptors, SR 95531 (5 μM) and CGP 55845 hydrochloride (1 μM) to block $GABA_A$ and $GABA_B$ receptors, dihydro-β-erythroidine hydrobromide (1 μM) and scopolamine (0.2 μM) to block nAChRs as well as muscarinic AChRs (mAChRs). Medial Hb ChNs typically have sparse spontaneous excitatory and inhibitory postsynaptic currents (Fig. 3D). Perfusion of the transmitter antagonist cocktail, which abolished these sparse postsynaptic currents (3/3 cells), did not alter the tonic firing rate of mHb ChNs in either control-sleep or SF groups (SF x antagonists interaction: $F_{(1, 16)} = 0.023$, $p = 0.882$; main effect of antagonists cocktail: $F_{(1, 16)} = 0.045$, $p = 0.835$; main effect of SF: $F_{(1, 16)} = 9.667$, $p = 0.007$; two-way RM ANOVA with Sidak posttest; Fig. 3D). Importantly, the SF-induced increase in tonic action potential firing remained intact in the presence of the antagonist cocktail, indicating that the SF-induced hyperactivity is not mediated by these fast synaptic transmissions (SF effect in cocktail: $p = 0.031$, n = 9/4-6, two-way ANOVA with Sidak posttest; Fig. 3D). Similarly, the firing regularity also was not affected upon application of the antagonist cocktail, where SF-induced increase in firing regularity persisted ($CV_{interval}$: SF x antagonists interaction, $F_{(1, 16)} = 2.033$, $p = 0.173$; main effect of antagonists cocktail: $F_{(1, 16)} = 0.079$, $p = 0.783$; main effect of SF, $F_{(1, 16)} = 6.097$, $p = 0.025$; two-way RM ANOVA with Sidak posttest; Fig. 3D). We thus did not pursue the impact of synaptic inputs but focused on the membrane properties of mHb ChNs.

Background K⁺ channels in SF-induced increase of tonic firing in mHb ChNs

Several classes of K^+ channels are expressed in mHb ChNs in high abundance, which are sensitive to intracellular environment and regulate the resting membrane potential. Among these candidates, the small-conductance calcium-activated potassium channels (SK) subtypes SK2 and SK3 are highly expressed in the rodent mHb[41], and SK3 activity has been shown to regulate the circadian rhythm of mHb neurons basal firing in young animals[42]. Indeed, an SK2/3 channel enhancer NS 309 (20 μM) in the presence of the cocktail antagonists potently decreased the tonic firing of mHb ChNs in both control-sleep and SF groups (SF x NS 309 interaction: $F_{(1, 10)} = 2.427$, $p = 0.150$; main effect of SF: $F_{(1, 10)} =$

16.78, $p = 0.002$; main effect of NS 309: $F_{(1, 10)} = 65.72$, $p < 0.001$; two-way RM ANOVA with Sidak posttest; Fig. 4A), confirming functional expression of SK2/3 in the mouse mHb ChNs in both treatment conditions. It is noteworthy that the firing regularity was reduced by NS 309 ($CV_{interval}$: SF x NS 309 interaction, $F_{(1, 8)} = 3.003$, $p = 0.121$; main effect of NS 309: $F_{(1, 8)} = 7.259$, $p = 0.027$; 1 cell from each group was excluded from CV analysis because of a complete lack of firing in NS 309; two-way RM ANOVA with Sidak posttest). To test whether the basal SK channel activity mediates the low firing frequency under control-sleep conditions, as well as the opposite possibility that SK channel closure may induce depolarization block thus reduce action potential firing in mHb ChNs[42], we applied SK2 (UCL 1684, 1 μM) and SK3-selective antagonists (TRAM 39, 1 μM) following either control-sleep or SF. Although these antagonists effectively reversed the NS 309 effect (Fig. 4A; 7/7 cells), neither of these antagonists, combined (Fig. 4B) or separately (Fig. 4C), affected the basal tonic firing rate in mHb ChNs from control-sleep or SF mice (UCL +TRAM: SF x drugs interaction, $F_{(1, 16)} = 0.654$, $p = 0.431$; main effect of SF, $F_{(1, 16)} = 9.341$, $p = 0.008$; main effect of drugs, $F_{(1, 16)} = 0.270$, $p = 0.610$; two-way RM ANOVA with Sidak posttest. UCL or TRAM separate: control-sleep, $F_{(2, 49)} = 0. 0322$, $p = 0.968$; SF, $F_{(2, 47)} = 0.162$, $p = 0.851$; one-way ANOVA with Tukey posttest). Application of combined SK2/3 antagonists also did not alter the firing regularity in mHb ChNs in control-sleep or SF mice ($CV_{interval}$: SF x drugs interaction, $F_{(1, 16)} = 0.648$, $p = 0.434$; main effect of drugs, $F_{(1, 16)} = 2.568$, $p = 0.130$; two-way RM ANOVA with Sidak posttest). These results exclude the involvement of SK2 and SK3 in mediating the SF-induced hyperactivity of mHb ChNs.

We then considered K_{2P} channels, which contribute to the resting K^+ conductance and regulate the resting membrane potential[43, 44]. Two main types of K_{2P} channels, TWIK-1 (KCNK1) and TASK-3 (KCNK9), are expressed at high levels in the rat mHb[45]. These channels are not voltage-gated, but are sensitive to extracellular and/or intracellular pH[43, 44, 46]. Indeed, switching a HEPES-based aCSF bath from pH 7.3 to pH 6.5, which should predominantly inhibit TASK-3 channels[43, 46–48] and prevent them from hyperpolarizing the membrane potential, enhanced the tonic action potential firing in mHb ChNs ($F_{(2, 117)} = 3.525$, $p = 0.03$, one-way ANOVA with Dunnett posttest; Fig. 5A). By contrast, TWIK-1 channels are expected to be only modestly affected by extracellular acidification over this pH range (7.3 to 6.5), and possibly to have increased activation (i.e. hyperpolarization) around pH 6.5[49], thus would not support the acidification-induced increase in firing. Therefore, these results led us to test whether TASK-3 channels contribute to the SF-induced increase in tonic action potential firing in mHb ChNs. We first confirmed TASK-3 expression in the mouse mHb by RNAscope *in situ* hybridization, using a selective TASK-3 (Kcnk9) probe to detect TASK-3 mRNA signals (**Methods**; Fig. 5B). Next, we compared the resting membrane potential of mHb ChNs between control-sleep and SF mice upon application of a TASK-3-selective antagonist PK-THPP (1 μM). There was a significant SF x drug interaction ($F_{(1, 36)} = 7.236$, $p = 0.011$; two-way ANOVA with Tukey posttest; Fig. 5C). In control-sleep group, PK-THPP significantly depolarized the resting membrane potential in mHb ChNs ($p = 0.006$, n = 11–13/6), indicating TASK-3 as a key substrate maintaining the relatively hyperpolarized resting membrane potential. By contrast, in SF mice, application of PK-THPP did not change the resting membrane potential ($p = 0.932$, n = 8/4), suggesting reduced TASK-3 activity following SF. This is consistent with

the more depolarized resting membrane potential in SF mice ($p = 0.019$, n = 8–13/4–6, 6–8-week-old mice, Fig. 5C; also see 12–16-week-old mice, Fig. 2C). Finally, application of PK-THPP in control-sleep group mimicked, as well as occluded, the SF effect (control-sleep in PK-THPP compared to SF: $p = 0.999$; compared to SF in PK-THPP: $p = 0.880$, n = 8–11/4–6; two-way ANOVA followed by Tukey posttest), suggesting that TASK-3 channels mediate SF-induced depolarization of the resting membrane potential in mHb ChNs.

To test whether TASK-3 channels may underlie SF-induced hyperactivity of mHb ChNs, we compared the tonic firing of mHb ChNs between control-sleep and SF mice upon PK-THPP application. There was a significant SF x drug interaction ($F_{(1, 13)} = 14.26$, $p = 0.002$, two-way RM ANOVA). In control-sleep mice, PK-THPP increased the firing rate in mHb ChNs ($p = 0.0001$, n = 7/6, Sidak posttest), reaching the levels of SF mice ($p = 0.920$, n = 7–8/4–5; two-way ANOVA followed by Tukey posttest). By contrast, PK-THPP application did not affect the tonic firing rate in the SF group ($p = 0.278$, n = 8/5, Sidak posttest; Fig. 5D). Furthermore, the lack of PK-THPP effect in the SF group was not because that the tonic action potential firing had reached the maximal level, since the tonic firing in the SF group could be further increased by raising extracellular K^+ concentrations to 10–15 mM (mean ± SEM: normal K^+, 4.10 ± 0.30 Hz; high K^+, 5.91 ± 0.46 Hz; $p = 0.024$, n = 6/3, two-tailed paired t test; Fig. 5D), a manipulation that potently depolarizes the resting membrane potential. These results provide further support that TASK-3 channel activity is compromised following SF, resulting in hyperactivity of mHb ChNs. In addition to changing the tonic firing rate, application of PK-THPP also enhanced the firing regularity by decreasing $CV_{interval}$ in control-sleep group but not in SF group (SF x PK-THPP interaction: $F_{(1, 13)} = 2.884$, $p = 0.115$; PK-THPP effect in control-sleep: $p = 0.021$, n = 7/6; PK-THPP effect in SF: $p = 0.630$, n = 8/5; two-way RM ANOVA followed by Sidak posttest; control-sleep in PK-THPP compared to SF: $p = 0.606$, n = 7–8/4–5; two-way ANOVA followed by Tukey posttest; Fig. 5D). Thus, inhibition of TASK-3 channels in control-sleep group mimicked the SF effects on the resting membrane potential, firing rate, and firing regularity, whereas these effects of TASK-3 inhibition were occluded in the SF group. Together, these results suggest that TASK-3 is a key molecular target for SF to regulate mHb ChN firing.

Finally, we plotted the relationship between the firing frequency and $CV_{interval}$ of all recorded mHb ChNs from control-sleep group (without and with TASK-3 inhibition) and SF group (Fig. 5E). We first established the basal relationship using data from the control-sleep group in the absence of TASK-3 blocker, which exhibited an inverse correlation, best fit by Power function $y = 0.6x^{-0.9}$ ($R^2 = 0.923$). This plot revealed a unique property of mHb ChNs such that those that fired at higher frequencies exhibited higher regularity of firing. Further analysis showed that this relationship was preserved in SF mice, albeit shifted toward higher frequency and lower $CV_{interval}$. Moreover, this SF effect was mimicked by TASK-3 inhibition in the control-sleep group. Together, these results suggest a dual function of TASK-3 in regulating mHb ChNs firing frequency as well as regularity, and further support the engagement of TASK-3 in SF-induced alterations of mHb ChNs activity.

Discussion

Sleep disturbance disrupts physiological homeostasis and alters the emotional and motivational state[1–6]. The mHb cholinergic outputs play multifaceted roles in regulating mood, emotion, motivation, and reward[14]. Here we show that chronic REM SF induces hyperactivity of mHb cholinergic projection neurons through regulating K_{2P} channels TASK-3. These results demonstrate a novel molecular substrate through which sleep disturbance may impact emotion regulation.

REM sleep fragmentation

SF, and especially REM SF, is one of the most robust signatures in insomnia[50]. Our SF procedure recapitulates this important aspect of insomnia. Interestingly, we were able to achieve a predominant REM SF without changes in total NREM sleep, NREM episode durations, transitions, or NREM signature waveforms (Fig. 1). This REM-selectivity may be due to the design of our treadmill system and the SF schedule, which produces mild disturbances (see Methods). And REM sleep, being a more aroused brain state than NREM, may be more prone to disturbance[51]. Indeed, we previously showed that in rats undergoing withdrawal from repeated cocaine use, REM sleep was selectively disrupted using an similar treadmill procedure[23]. Thus, our treadmill system and SF procedure provide a new means to manipulate REM sleep in addition to the traditional methods (i.e., flowerpot or multiple platform method etc.) or EEG/EMG-based methods[27, 52].

Neurotransmitter receptors, SKs, and TASK-3 in mediating the SF effects

The mHb receives a variety of neurotransmitter and neuromodulator inputs[14]. Although many of these inputs may affect mHb ChNs firing upon receptor activation, most of the receptors under basal slice conditions appear not to be actively involved in setting the tonic firing tone. For example, mHb ChNs basal firing in slices are not affected by inhibition of AMPA and NMDA types of glutamate receptors, $GABA_A$ and $GABA_B$ receptors, or n/mACh receptors (Fig. 3). Neither was mHb ChNs basal firing affected by activation of histamine receptors, perhaps reflecting low receptor expression levels (Fig. 3). Apparently, we have not tested all potential neuromodulator systems exhaustively. For example, the mHb neural excitability may be modulated by peptides via G-protein signaling[53]. In addition, the mHb receives monoaminergic inputs from the ventral tegmental area and raphe[14], and it remains to be determined whether dopamine, norepinephrine, and serotonin may regulate the tonic action potential firing in mHb ChNs and contribute to the SF-induced hyperactivity.

It was previously shown that SK channel activation hyperpolarizes mHb neurons and reduces tonic action potential firing in young mice[42]. The same study also showed that activating SK channels can sometimes reduce depolarization block and thus revive firing in mHb neurons. We observed that although activation of SK channels strongly suppresses the spontaneous firing in mHb ChNs in both control-sleep and SF groups, inhibition of SK channels does not change the tonic firing rate in either group (Fig. 4). It is possible that under our basal conditions SK channels are mostly not active, thus occluding the effects of SK channel blockers. There could also be differences in basal SK channel activity levels between age groups and circadian times[42].

TASK-3 channel inhibition occluded SF-induced changes in mHb ChNs, including resting membrane potential, tonic firing frequency, and firing regularity (Fig. 5C,D), suggesting that TASK-3 is targeted by SF to regulate mHb ChNs firing. It is expected that SF-induced suppression of TASK-3 activity would lead to a reduction of the background potassium leak conductance, thus resulting in an increase of the membrane resistance. However, whole-cell recordings failed to detect such a change. Additionally, the SF-induced increase in tonic action potential firing was also not observed under whole-cell configurations. One explanation is that the resting membrane potential is sensitive to changes in intracellular K^+, and/or TASK-3 is sensitive to cytosolic microenvironment – including G-protein signaling and intracellular pH[54, 55]. Therefore, intracellular dialysis under the whole-cell recording configuration may normalize intracellular K^+ and pH, as well as disrupt G-protein signaling, and thus diminishes the potential differences. While the number of TASK-3 channels as well as the single channel conductance can also be affected by SF, an intriguing possibility is that SF decreases TASK-3 channel activity via G-protein signaling and/or intracellular acidification.

It is noteworthy that the TASK-3 channels in mHb ChNs appear not to be sensitive to histamine inhibition, since histamine application did not increase mHb ChN basal firing whereas TASK-3 inhibition did (Figs. 3,5). This is in contrast to the previous observation that histamine effectively inhibits TASK channels in basal forebrain cholinergic neurons via histamine receptor activation[56]. One explanation may be the low expression levels of histamine receptors: mHb ChNs do not appear to express histamine H1 receptors, and have low expressions of H2 and H3 receptors[36–38]. Another possibility is that TASK sensitivity to histamine may be dependent on the channel compositions that vary between different brain regions and cell types. For example, homomeric TASK-3 channels in striatal cholinergic interneurons are not sensitive to histamine inhibition, even in the presence of functional H1 histamine receptors[34, 57]. In mHb ChNs, there are high expressions of at least two types of K_{2P} channels, TASK-3 and TWIK-1[45]. The two K_{2P} channels may interact to form heteromeric channels as well as homomeric ones[58, 59], which may exhibit unique pharmacology. Thus, low expressions of histamine receptors as well as K_{2P} channel compositions may render mHb ChNs' pace-making activity insensitive to histamine.

TASK-3 regulation of firing frequency and regularity

TASK-3 as a background "leak" potassium channel may shape action potential firing in three prominent ways: (i) it sets the resting membrane potential and regulates the driving force for action potential initiation; (ii) it contributes to membrane conductance and thus affects the time constant for membrane charging/discharging; (iii) it facilitates membrane repolarization and action potential termination, which is critical during high-frequency trains[60, 61]. Thus, reduced TASK-3 activity may either increase firing rate by depolarizing the resting membrane potential, or decrease firing during high frequency trains by reducing membrane repolarization and delaying the recovery of voltage-gated sodium channels. On the other hand, how TASK-3 may regulate action potential firing regularity is less well understood. We found that the mHb ChNs exhibit ~0.5–10 Hz basal firing frequency in slice preparations, with an inverse correlation between the firing frequency and $CV_{interval}$ (Fig. 5E). This is remarkably similar to a frequency-$CV_{interval}$ relation observed in the rat striatal

cholinergic neurons[62]. Interestingly in striatal cholinergic neurons, artificially reducing hyperpolarization of the membrane potential leads to an increase in firing frequency accompanied by enhanced firing regularity (decreased $CV_{interval}$)[62]. This is consistent with our findings in mHb ChNs that TASK-3 inhibition (reducing potassium currents) induces similar changes (Fig. 5E). Although during high frequency trains the closure of potassium channels may increase frequency at the cost of firing regularity[60], at the relatively low basal firing frequency range, a positive correlation between firing frequency and regularity applies to mHb ChNs in the control-sleep group, as well as following TASK-3 inhibition or SF (Fig. 5E).

Behavioral indications

REM sleep is especially important for emotional memory and mood regulations[7, 8, 63, 64]. Thus, it is interesting to note that mHb ChNs are sensitive to selective REM sleep disturbance. Could mHb ChNs mediate some of the REM sleep effects on mood regulation?

Indeed, the mHb is uniquely positioned for mediating sleep-mood regulations – it relays information from limbic forebrain to midbrain monoaminergic centers. Activity of mHb regulates, or is regulated by, sleep, circadian rhythms, stress, and reward[14, 65]. Selective oblation of mHb neurons or suppression of mHb ChN transmission leads to a variety of maladaptive behaviors affecting learning & memory, fear extinction, as well as nicotine addiction[15, 16, 18]. On the other hand, increasing mHb ChN activity or enhancing cholinergic transmission onto downstream IPN neurons worsens drug withdrawal-induced anxiety and induces drug reinstatement[17, 66]. It remains to be determined whether the REM SF-induced increase in mHb ChNs tonic firing may contribute to the behavioral maladaptations of REM sleep disturbance, including changes in anxiety levels, depressive mood, and drug withdrawal and relapse.

Acknowledgement:

References

1. Medic G, Wille M, Hemels ME. Short- and long-term health consequences of sleep disruption. Nat Sci Sleep 2017; 9: 151–161. [PubMed: 28579842]

2. Finan PH, Quartana PJ, Smith MT. The Effects of Sleep Continuity Disruption on Positive Mood and Sleep Architecture in Healthy Adults. Sleep 2015; 38(11): 1735–1742. [PubMed: 26085289]

3. Logan RW, Hasler BP, Forbes EE, Franzen PL, Torregrossa MM, Huang YH et al. Impact of Sleep and Circadian Rhythms on Addiction Vulnerability in Adolescents. Biol Psychiatry 2018; 83(12): 987–996. [PubMed: 29373120]

4. Meerlo P, Havekes R, Steiger A. Chronically restricted or disrupted sleep as a causal factor in the development of depression. Curr Top Behav Neurosci 2015; 25: 459–481. [PubMed: 25646723]

5. Krystal AD. Psychiatric disorders and sleep. Neurol Clin 2012; 30(4): 1389–1413. [PubMed: 23099143]

6. Anderson KN, Bradley AJ. Sleep disturbance in mental health problems and neurodegenerative disease. Nat Sci Sleep 2013; 5: 61–75. [PubMed: 23761983]

7. Palmer CA, Alfano CA. Sleep and emotion regulation: An organizing, integrative review. Sleep Med Rev 2017; 31: 6–16. [PubMed: 26899742]

8. Goldstein AN, Walker MP. The role of sleep in emotional brain function. Annu Rev Clin Psychol 2014; 10: 679–708. [PubMed: 24499013]

9. Krause AJ, Simon EB, Mander BA, Greer SM, Saletin JM, Goldstein-Piekarski AN et al. The sleep-deprived human brain. Nat Rev Neurosci 2017; 18(7): 404–418. [PubMed: 28515433]

10. Hall M, Levenson J, Hasler B. Sleep and Emotion. In: Morin CM, Espie CA (eds). The Oxford Handbook of Sleep and Sleep Disorders Oxford University Press 2012.

11. Gruber R, Cassoff J. The interplay between sleep and emotion regulation: conceptual framework empirical evidence and future directions. Curr Psychiatry Rep 2014; 16(11): 500. [PubMed: 25200984]

12. Minkel JD, McNealy K, Gianaros PJ, Drabant EM, Gross JJ, Manuck SB et al. Sleep quality and neural circuit function supporting emotion regulation. Biol Mood Anxiety Disord 2012; 2: 22. [PubMed: 23216889]

13. Simon EB, Oren N, Sharon H, Kirschner A, Goldway N, Okon-Singer H et al. Losing Neutrality: The Neural Basis of Impaired Emotional Control without Sleep. The Journal of neuroscience: the official journal of the Society for Neuroscience 2015; 35(38): 13194–13205. [PubMed: 26400948]

14. Viswanath H, Carter AQ, Baldwin PR, Molfese DL, Salas R. The medial habenula: still neglected. Front Hum Neurosci 2013; 7: 931. [PubMed: 24478666]

15. Zhang J, Tan L, Ren Y, Liang J, Lin R, Feng Q et al. Presynaptic Excitation via GABAB Receptors in Habenula Cholinergic Neurons Regulates Fear Memory Expression. Cell 2016; 166(3): 716–728. [PubMed: 27426949]

16. Kobayashi Y, Sano Y, Vannoni E, Goto H, Suzuki H, Oba A et al. Genetic dissection of medial habenula-interpeduncular nucleus pathway function in mice. Front Behav Neurosci 2013; 7: 17. [PubMed: 23487260]

17. Lopez AJ, Jia Y, White AO, Kwapis JL, Espinoza M, Hwang P et al. Medial habenula cholinergic signaling regulates cocaine-associated relapse-like behavior. Addict Biol 2018.

18. Fowler CD, Lu Q, Johnson PM, Marks MJ, Kenny PJ. Habenular alpha5 nicotinic receptor subunit signalling controls nicotine intake. Nature 2011; 471(7340): 597–601. [PubMed: 21278726]

19. Frahm S, Slimak MA, Ferrarese L, Santos-Torres J, Antolin-Fontes B, Auer S et al. Aversion to nicotine is regulated by the balanced activity of beta4 and alpha5 nicotinic receptor subunits in the medial habenula. Neuron 2011; 70(3): 522–535. [PubMed: 21555077]

20. Han S, Yang SH, Kim JY, Mo S, Yang E, Song KM et al. Down-regulation of cholinergic signaling in the habenula induces anhedonia-like behavior. Sci Rep 2017; 7(1): 900. [PubMed: 28420875]

21. Yamaguchi T, Danjo T, Pastan I, Hikida T, Nakanishi S. Distinct roles of segregated transmission of the septo-habenular pathway in anxiety and fear. Neuron 2013; 78(3): 537–544. [PubMed: 23602500]

22. Tallini YN, Shui B, Greene KS, Deng KY, Doran R, Fisher PJ et al. BAC transgenic mice express enhanced green fluorescent protein in central and peripheral cholinergic neurons. Physiol Genomics 2006; 27(3): 391–397. [PubMed: 16940431]

23. Chen B, Wang Y, Liu X, Liu Z, Dong Y, Huang YH. Sleep Regulates Incubation of Cocaine Craving. The Journal of neuroscience: the official journal of the Society for Neuroscience 2015; 35(39): 13300–13310. [PubMed: 26424879]

24. Liu Z, Wang Y, Cai L, Li Y, Chen B, Dong Y et al. Prefrontal Cortex to Accumbens Projections in Sleep Regulation of Reward. The Journal of neuroscience: the official journal of the Society for Neuroscience 2016; 36(30): 7897–7910. [PubMed: 27466335]

25. Winters BD, Huang YH, Dong Y, Krueger JM. Sleep loss alters synaptic and intrinsic neuronal properties in mouse prefrontal cortex. Brain research 2011; 1420: 1–7. [PubMed: 21962531]

26. Ting JT, Daigle TL, Chen Q, Feng G. Acute brain slice methods for adult and aging animals: application of targeted patch clamp analysis and optogenetics. Methods Mol Biol 2014; 1183: 221–242. [PubMed: 25023312]

27. Colavito V, Fabene PF, Grassi-Zucconi G, Pifferi F, Lamberty Y, Bentivoglio M et al. Experimental sleep deprivation as a tool to test memory deficits in rodents. Frontiers in systems neuroscience 2013; 7: 106. [PubMed: 24379759]

28. Malisch JL, Breuner CW, Gomes FR, Chappell MA, Garland T Jr. Circadian pattern of total and free corticosterone concentrations, corticosteroid-binding globulin, and physical activity in mice selectively bred for high voluntary wheel-running behavior. General and comparative endocrinology 2008; 156(2): 210–217. [PubMed: 18329645]

29. Aizawa H, Kobayashi M, Tanaka S, Fukai T, Okamoto H. Molecular characterization of the subnuclei in rat habenula. J Comp Neurol 2012; 520(18): 4051–4066. [PubMed: 22700183]

30. Cuello AC, Emson PC, Paxinos G, Jessell T. Substance P containing and cholinergic projections from the habenula. Brain research 1978; 149(2): 413–429. [PubMed: 352479]

31. Choi K, Lee Y, Lee C, Hong S, Lee S, Kang SJ et al. Optogenetic activation of septal GABAergic afferents entrains neuronal firing in the medial habenula. Sci Rep 2016; 6: 34800. [PubMed: 27703268]

32. Shih PY, Engle SE, Oh G, Deshpande P, Puskar NL, Lester HA et al. Differential expression and function of nicotinic acetylcholine receptors in subdivisions of medial habenula. The Journal of neuroscience: the official journal of the Society for Neuroscience 2014; 34(29): 9789–9802. [PubMed: 25031416]

33. Dao DQ, Perez EE, Teng Y, Dani JA, De Biasi M. Nicotine enhances excitability of medial habenular neurons via facilitation of neurokinin signaling. The Journal of neuroscience: the official journal of the Society for Neuroscience 2014; 34(12): 4273–4284. [PubMed: 24647947]

34. Bell MI, Richardson PJ, Lee K. Histamine depolarizes cholinergic interneurones in the rat striatum via a H(1)-receptor mediated action. British journal of pharmacology 2000; 131(6): 1135–1142. [PubMed: 11082121]

35. Gorelova N, Reiner PB. Histamine depolarizes cholinergic septal neurons. Journal of neurophysiology 1996; 75(2): 707–714. [PubMed: 8714646]

36. Palacios JM, Wamsley JK, Kuhar MJ. The distribution of histamine H1-receptors in the rat brain: an autoradiographic study. Neuroscience 1981; 6(1): 15–37. [PubMed: 6111763]

37. Pillot C, Heron A, Cochois V, Tardivel-Lacombe J, Ligneau X, Schwartz JC et al. A detailed mapping of the histamine H(3) receptor and its gene transcripts in rat brain. Neuroscience 2002; 114(1): 173–193. [PubMed: 12207964]

38. Vizuete ML, Traiffort E, Bouthenet ML, Ruat M, Souil E, Tardivel-Lacombe J et al. Detailed mapping of the histamine H2 receptor and its gene transcripts in guinea-pig brain. Neuroscience 1997; 80(2): 321–343. [PubMed: 9284338]

39. Sheffield EB, Quick MW, Lester RA. Nicotinic acetylcholine receptor subunit mRNA expression and channel function in medial habenula neurons. Neuropharmacology 2000; 39(13): 2591–2603. [PubMed: 11044729]

40. Bischoff S, Leonhard S, Reymann N, Schuler V, Shigemoto R, Kaupmann K et al. Spatial distribution of GABA(B)R1 receptor mRNA and binding sites in the rat brain. J Comp Neurol 1999; 412(1): 1–16. [PubMed: 10440706]

41. Stocker M, Pedarzani P. Differential distribution of three Ca(2+)-activated K(+) channel subunits, SK1, SK2, and SK3, in the adult rat central nervous system. Molecular and cellular neurosciences 2000; 15(5): 476–493. [PubMed: 10833304]

42. Sakhi K, Belle MD, Gossan N, Delagrange P, Piggins HD. Daily variation in the electrophysiological activity of mouse medial habenula neurones. The Journal of physiology 2014; 592(4): 587–603. [PubMed: 24247982]

43. O'Connell AD, Morton MJ, Hunter M. Two-pore domain K+ channels-molecular sensors. Biochim Biophys Acta 2002; 1566(1–2): 152–161. [PubMed: 12421546]

44. Braun AP. Two-pore domain potassium channels: variation on a structural theme. Channels (Austin) 2012; 6(3): 139–140. [PubMed: 22699405]

45. Talley EM, Solorzano G, Lei Q, Kim D, Bayliss DA. Cns distribution of members of the two-pore-domain (KCNK) potassium channel family. The Journal of neuroscience: the official journal of the Society for Neuroscience 2001; 21(19): 7491–7505. [PubMed: 11567039]

46. Lesage F, Barhanin J. Molecular physiology of pH-sensitive background K(2P) channels. Physiology (Bethesda) 2011; 26(6): 424–437. [PubMed: 22170960]

47. Bayliss DA, Barhanin J, Gestreau C, Guyenet PG. The role of pH-sensitive TASK channels in central respiratory chemoreception. Pflugers Arch 2015; 467(5): 917–929. [PubMed: 25346157]

48. Meadows HJ, Randall AD. Functional characterisation of human TASK-3, an acid-sensitive two-pore domain potassium channel. Neuropharmacology 2001; 40(4): 551–559. [PubMed: 11249964]

49. Chatelain FC, Bichet D, Douguet D, Feliciangeli S, Bendahhou S, Reichold M et al. TWIK1, a unique background channel with variable ion selectivity. Proc Natl Acad Sci U S A 2012; 109(14): 5499–5504. [PubMed: 22431633]

50. Baglioni C, Regen W, Teghen A, Spiegelhalder K, Feige B, Nissen C et al. Sleep changes in the disorder of insomnia: a meta-analysis of polysomnographic studies. Sleep Med Rev 2014; 18(3): 195–213. [PubMed: 23809904]

51. Ermis U, Krakow K, Voss U. Arousal thresholds during human tonic and phasic REM sleep. Journal of sleep research 2010; 19(3): 400–406. [PubMed: 20477954]

52. Gulyani S, Majumdar S, Rapid BNM eye movement sleep and significance of its deprivation studies - A review. Sleep and Hypnosis 2000; 2(2): 49–68.

53. Tuesta LM, Chen Z, Duncan A, Fowler CD, Ishikawa M, Lee BR et al. GLP-1 acts on habenular avoidance circuits to control nicotine intake. Nat Neurosci 2017; 20(5): 708–716. [PubMed: 28368384]

54. Kim Y, Bang H, Kim D. TASK-3, a new member of the tandem pore K(+) channel family. J Biol Chem 2000; 275(13): 9340–9347. [PubMed: 10734076]

55. Talley EM, Bayliss DA. Modulation of TASK-1 (Kcnk3) and TASK-3 (Kcnk9) potassium channels: volatile anesthetics and neurotransmitters share a molecular site of action. J Biol Chem 2002; 277(20): 17733–17742. [PubMed: 11886861]

56. Vu MT, Du G, Bayliss DA, Horner RL. TASK Channels on Basal Forebrain Cholinergic Neurons Modulate Electrocortical Signatures of Arousal by Histamine. The Journal of neuroscience: the official journal of the Society for Neuroscience 2015; 35(40): 13555–13567. [PubMed: 26446210]

57. Berg AP, Bayliss DA. Striatal cholinergic interneurons express a receptor-insensitive homomeric TASK-3-like background K+ current. Journal of neurophysiology 2007; 97(2): 1546–1552. [PubMed: 17167057]

58. Cho CH, Hwang EM, Park JY. Emerging Roles of TWIK-1 Heterodimerization in the Brain. Int J Mol Sci 2017; 19(1).

59. Plant LD, Zuniga L, Araki D, Marks JD, Goldstein SA. SUMOylation silences heterodimeric TASK potassium channels containing K2P1 subunits in cerebellar granule neurons. Sci Signal 2012; 5(251): ra84. [PubMed: 23169818]

60. Brickley SG, Aller MI, Sandu C, Veale EL, Alder FG, Sambi H et al. TASK-3 two-pore domain potassium channels enable sustained high-frequency firing in cerebellar granule neurons. The Journal of neuroscience: the official journal of the Society for Neuroscience 2007; 27(35): 9329–9340. [PubMed: 17728447]

61. Goldstein SA, Bockenhauer D, O'Kelly I, Zilberberg N. Potassium leak channels and the KCNK family of two-P-domain subunits. Nat Rev Neurosci 2001; 2(3): 175–184. [PubMed: 11256078]

62. Bennett BD, Callaway JC, Wilson CJ. Intrinsic membrane properties underlying spontaneous tonic firing in neostriatal cholinergic interneurons. The Journal of neuroscience: the official journal of the Society for Neuroscience 2000; 20(22): 8493–8503. [PubMed: 11069957]

63. Murkar ALA, De Koninck J. Consolidative mechanisms of emotional processing in REM sleep and PTSD. Sleep Med Rev 2018.

64. Groch S, Wilhelm I, Diekelmann S, Born J. The role of REM sleep in the processing of emotional memories: evidence from behavior and event-related potentials. Neurobiology of learning and memory 2013; 99: 1–9. [PubMed: 23123802]

65. Mathis V, Kenny PJ. From controlled to compulsive drug-taking: The role of the habenula in addiction. Neurosci Biobehav Rev 2018.

66. Zhao-Shea R, DeGroot SR, Liu L, Vallaster M, Pang X, Su Q et al. Increased CRF signalling in a ventral tegmental area-interpeduncular nucleus-medial habenula circuit induces anxiety during nicotine withdrawal. Nat Commun 2015; 6: 6770. [PubMed: 25898242]
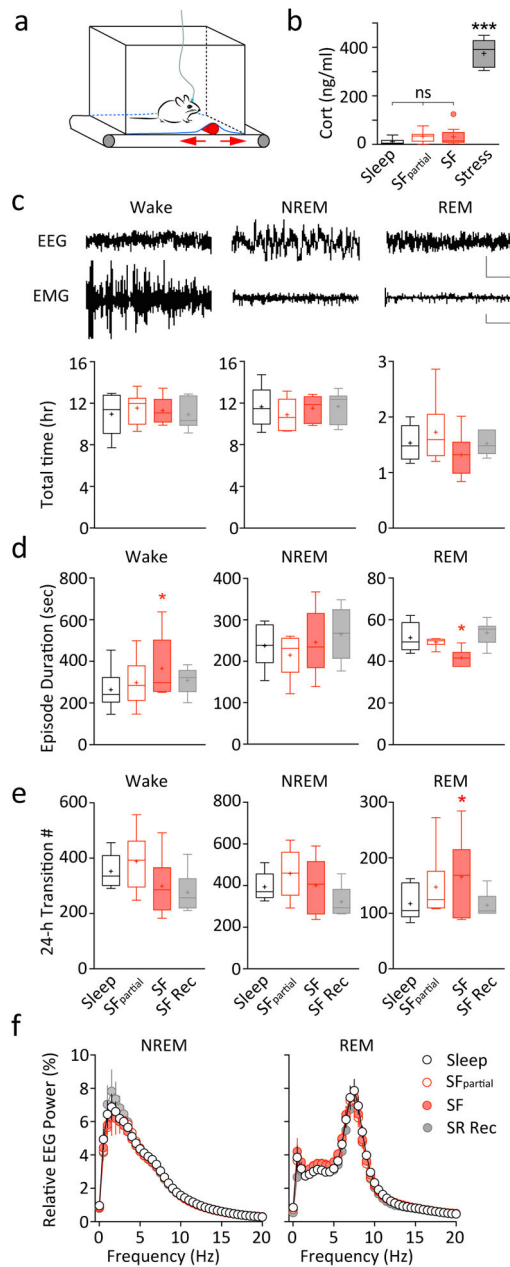
Fig. 1.

Sleep fragmentation in mice. **A** Design of the custom-made treadmill system used for SF. The treadmill system contains a programmable treadmill motor and belt; a bottomless housing cage on top with a flexible stainless-steel mesh floor covered with normal bedding; a cylinder-shaped object affixed to the treadmill belt moving back and forth (*arrows*) underneath the cage floor to sleep-restrict the mice (detail see Methods). **B** Plasma corticosterone levels measured following control-sleep (Sleep), SF$_{partial}$, 5 days of SF (SF), or acute physical restraint stress (Stress), showing a lack of change following SF, and an increase upon acute stress. n = 7–9 each. **C-F** Sleep measurements across four conditions: Sleep, SF$_{partial}$, SF, and SF recovery (SF Rec). **C** The 24-hr total time spent in wakefulness,

NREM, or REM sleep were not different. *Top*, example EEG and EMG traces showing wakefulness, NREM, and REM states. Scale bars = 800 μV (EEG), 1000 μV (EMG), 2 s. **D** Average wakefulness bout duration was increased during SF, and REM sleep episode duration was selectively decreased during SF. **E** Number of state transitions showed an increase selectively in REM sleep initiation during SF. **F** There were no changes in the EEG power spectra during NREM or REM episodes. n = 6 each. Values are presented in box-and-whiskers plots in the style of Tukey. * $p < 0.05$, *** $p < 0.001$, ns = not significant
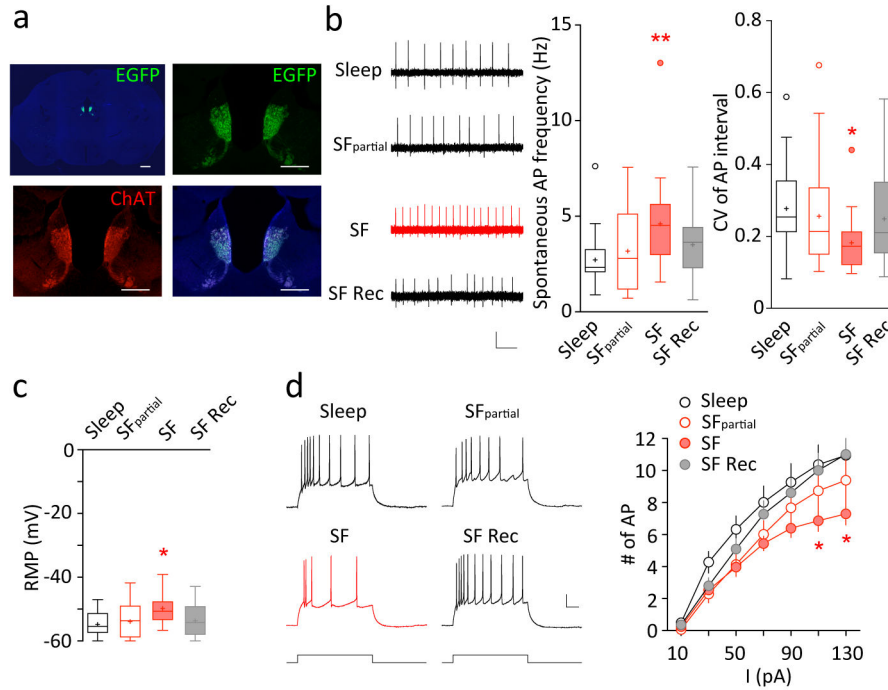
Fig. 2.
SF-induced increase in mHb ChNs tonic firing in slices. **A** Strong EGFP signal (green) in mHb ChAT-immunoreactive (red) ChNs from a ChAT[BAC]-EGFP mouse. Medial Hb EGFP and ChAT signals showed complete overlap, both of which were concentrated at the ventral two-thirds of mHb. Scale bars = 500 μm, 200 μm. **B** Examples and summaries showing tonic firing of mHb ChNs recorded under loose-patch configuration across four different conditions: control-sleep (n = 39/10), $SF_{partial}$ (n = 22/5), 5–7 days of SF (n = 31/9), and following SF recovery (n = 26/6). An increase in the tonic firing rate of mHb ChNs was observed selectively in the SF group. Scale bars = 0.2 mV, 500 ms. **C** Resting membrane potential (RMP) measured in mHb ChNs across the four conditions: control-sleep (n = 21/6), $SF_{partial}$ (n = 28/5), 5–7 days of SF (n = 22/6), and following SF recovery (n = 23/6). A more depolarized RMP was observed selectively in the SF group. ~12–16-week-old ChAT[BAC]-EGFP mice were used for this experiment. **D** Examples and summaries showing evoked action potentials recorded under whole-cell current-clamp configuration across the four conditions: control-sleep (n = 19/6), $SF_{partial}$ (n = 18/5), 5–7 days of SF (n = 21/6), and following SF recovery (n = 21/6). There was reduced action potential firing at high (110, 130 pA) current injections in the SF group, suggesting a modest decrease in membrane excitability at high firing frequencies (~20–30 Hz). Scale bars = 20 mV, 50 ms. Values are presented in box-and-whiskers plots in the style of Tukey (**B,C**), or mean ± SEM (**D**). * $p < 0.05$, ** $p < 0.01$
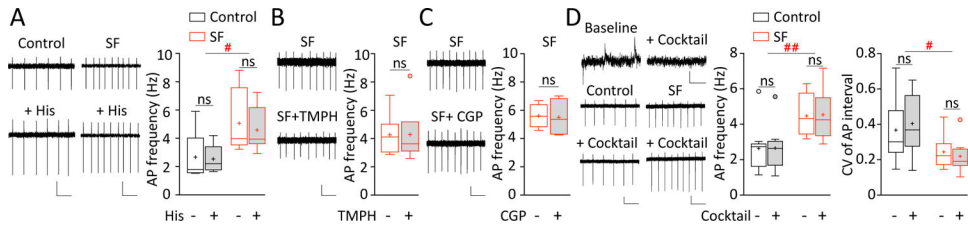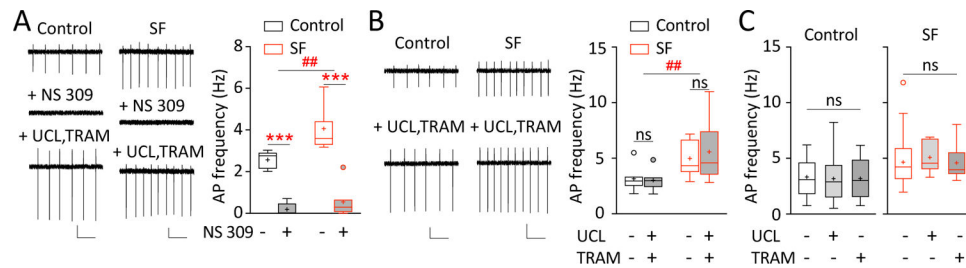
Fig. 3.

SF-induced increase in mHb ChNs tonic firing is not mediated by neurotransmitter receptors. **A** Examples and summaries showing that bath application of histamine (His; 10 µM) did not alter tonic firing rate in mHb ChNs in control-sleep or SF groups (n = 6/5 each). Scale bars = 50 pA, 200 pA, 500 ms. **B** Examples and summaries showing that bath application of pan-selective nAChR antagonist TMPH (1 µM) did not alter tonic firing rate in mHb ChNs in SF group (n = 6/4). Scale bars = 20 pA, 500 ms. **C** Examples and summaries showing that bath application of GABA$_B$ receptor selective antagonist CGP 55845 (CGP; 1 µM) did not alter tonic firing rate in mHb ChNs in SF group (n = 4/2). Scale bars = 20 pA, 500 ms. **D** *Top* An example showing that bath application of neurotransmitter receptor antagonist cocktail (NBQX 5 µM, D-AP5 50 µM, SR 95531 5 µM, and CGP 55845 hydrochloride 1 µM, dihydro-β-erythroidine hydrobromide 1 µM, and scopolamine 0.2 µM) eliminated spontaneous EPSCs and IPSCs (downward and upward deflections) recorded under whole-cell voltage-clamp mode. Scale bars = 10 pA, 200 ms. However, the antagonist cocktail did not alter the tonic firing frequency or firing regularity (shown as CV$_{interval}$) in mHb ChNs in control-sleep (n = 9/4) or SF groups (n = 9/6). Scale bars = 20 pA, 500 ms. Values are presented in box-and-whiskers plots in the style of Tukey. # $p < 0.05$, ## $p < 0.01$, ns = not significant

Fig. 4.
SF-induced increase in mHb ChNs tonic firing is not mediated by SK2 or SK3 channels. **A** Examples and summaries showing that bath application of SK2/3 channel enhancer NS 309 (20 μM) strongly suppressed tonic firing in mHb ChNs in both control-sleep and SF groups, an effect reversed by application of mixed SK2 selective antagonist UCL 1684 (UCL; 1 μM) and SK3 selective antagonist TRAM 39 (TRAM; 1 μM) (n = 5/3, 7/5). Scale bars = 50 pA, 500 ms; 20 pA, 500 ms. **B** Examples and summaries showing that bath application of UCL (1 μM) and TRAM (1 μM) together did not alter tonic firing rate in mHb ChNs in control-sleep or SF group (n = 7/5, 11/6). Scale bars = 50 pA, 500 ms. **C** Examples and summaries showing that bath application of UCL (1 μM) or TRAM (1 μM) separately did not alter tonic firing rate in mHb ChNs in control-sleep group (n = 17/5, 25/5, 11/5) or SF group (n = 27/5, 8/3, 8/5). Values are presented in box-and-whiskers plots in the style of Tukey. ** $p < 0.01$, *** $p < 0.001$, ## $p < 0.01$, ns = not significant
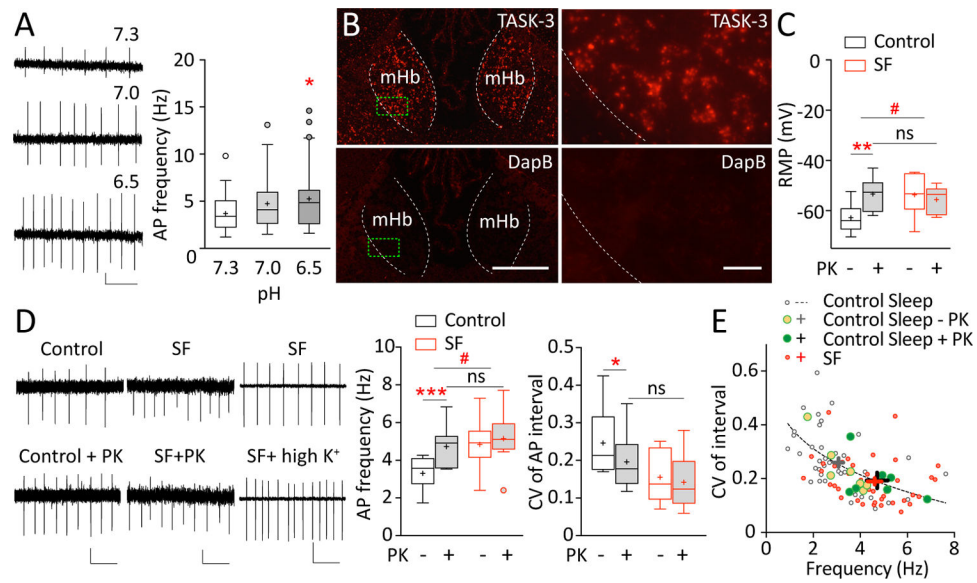
Fig. 5.

SF-induced increase in mHb ChNs tonic firing is partially mediated by K_{2P} channel TASK-3. **A** Examples and summaries showing an increase in tonic firing of mHb ChNs in acidic pH (n = 19/5). HEPES-buffered aCSF was adjusted to pH 7.3 (normal), 7.0, and 6.5 (acidic). Scale bars = 0.1 mV, 500 ms. **B** Expression of TASK-3 mRNA in the mouse mHb as revealed by RNAscope *in situ* hybridization, imaged under 10x and 40x magnifications. Selective Kcnk9 (TASK-3) probe was used and compared to hybridization using selective DapB probe (negative control). Green boxes represent the enlarged regions shown on right. Scale bars = 200 μm, 20 μm. **C** Summaries showing that bath application of TASK-3 selective antagonist PK-THPP (PK; 1 μM) led to depolarization of the resting membrane potential (RMP) in mHb ChNs in control-sleep group (n = 11–13/6) but not SF group (n = 8/4). ~6–8-week-old ChAT[BAC]-EGFP mice were used for this experiment. **D** Examples and summaries showing that bath application of TASK-3 selective antagonist PK-THPP (PK; 1 μM) increased the tonic firing rate and decreased $CV_{interval}$ in control-sleep group (n = 7/6) but not SF group (n = 8/5). In SF group, bath application of high-K^+ aCSF (10–15 mM) further enhanced tonic firing in mHb ChNs ($p = 0.024$, n = 6/3), suggesting that the lack of PK-THPP effect in the SF group was not because of a ceiling effect. Scale bars = 20 pA,10 pA, 100 pA; 500 ms. Values are presented in box-and-whiskers plots in the style of Tukey (**A-D**). **E** An inverse correlation between the firing frequency and $CV_{interval}$ was best fit by Power function $y = 0.6x^{-0.9}$ (based on control-sleep basal firing data; $R^2 = 0.923$; shown in dotted line). SF increased the firing frequency and reduced CV along the fit curve, suggesting enhanced firing regularity; these effects were recapitulated by TASK-3 inhibition in the control-sleep group. Group mean and SEM are indicated by the cross ("+") signs. * $p < 0.05$, ** $p < 0.01$, *** $p < 0.001$, # $p < 0.05$, ns = not significant

Table 1

Membrane properties and action potential parameters of mHb ChNs across four sleep conditions.

	Control Sleep	Control SF	SF	SF Recovery	
Number of cells/mice	18-21/6	16-28/5	20-22/6	18-23/6	
R_{in} at -10 pA (G)	1.55 ± 0.17	1.49 ± 0.15	1.87 ± 0.18	1.71 ± 0.15	
AP threshold (mV)	-38.5 ± 1.5	-36.6 ± 2.2	-35.8 ± 1.1	-34.9 ± 1.4	threshold
Spike amplitude (mV)	59.6 ± 3.3	57.0 ± 2.7	56.9 ± 2.8	57.9 ± 2.7	fAHP
fAHP amplitude (mV)	8.71 ± 0.66	10.45 ± 1.21	10.14 ± 1.18	10.81 ± 1.05	
mAHP amplitude (mV)	10.80 ± 1.14	11.61 ± 1.16	13.63 ± 0.97	13.28 ± 1.35	
AP rise time (ms)	0.56 ± 0.07	0.64 ± 0.10	0.53 ± 0.03	0.75 ± 0.10	mAHP
Rheobase I (pA)	26.8 ± 3.2	33.3 ± 2.9	27.1 ± 2.1	34.4 ± 4.3	
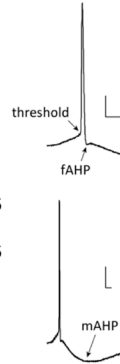
Abbreviations: AP, action potential; f(m)AHP, fast (medium) after hyperpolarization potential; Rheobase I: rheobase current; R_{in}, input resistance; scale bars = 10 ms, 10 mV.